IEEE Access
Multidisciplinary | Rapid Review | Open Access Journal

Received September 26, 2019, accepted October 17, 2019, date of publication October 28, 2019,
date of current version November 11, 2019.

Digital Object Identifier 10.1109/ACCESS.2019.2949746

Fault-Tolerant Dynamic Control of a Four-Wheel Redundantly-Actuated Mobile Robot

XIAOLONG ZHANG, YUANLONG XIE, LIQUAN JIANG, GEN LI, JIE MENG, AND YU HUANG
School of Mechanical Science and Engineering, Huazhong University of Science and Technology, Wuhan 430074, China

Corresponding author: Yu Huang (yuhuang_hust@163.com)

The work was supported in part by the DongGuan Innovative Research Team Program under Grant 201536000100031, in part by the China Postdoctoral Science Foundation under Grant 2019M650179, in part by the Hubei Technical Innovation Project under Grant 2018AAA027, and in part by the Guangdong Major Science and Technology Project under Grant 2019B090919003.

ABSTRACT Four-wheel redundantly-actuated mobile robot (FRMR) offers high controllability and maneuverability for automation applications. However, the robot dynamics and actuator failures are normally omitted in existing kinematic control schemes, which may lead to steering vibration and degraded robustness. To deal with these problems, a fault-tolerant dynamic control method is developed for precise trajectory tracking of the FRMR, which utilizes a two-level structure to cover the wheel-ground interactions and possible actuator failures. In the high level, with a novel fractional-order sliding mode control, this method offers an effective way to regulate the steering angle and eliminate the rotation chattering simultaneously. For the redundantly-actuated issue, a robust allocation solution is presented in the lower level to straightly determine optimal driving torques with full considerations of actuator failures and optimization efficiency. The convergence and stability of the achieved FRMR system are guaranteed theoretically. The experimental comparative results verify that higher tracking precision and enhanced robustness can be obtained using our proposed method.

INDEX TERMS Fault-tolerant dynamic control, four-wheel redundantly-actuated mobile robot, fractional-order sliding mode control, wheel-ground interactions.

I. INTRODUCTION

Due to the remarkable maneuverability, flexibility and dexterity, mobile robots have received a growing interest in broad applications, such as manufacturing, agriculture and outdoor exploration [1]–[3]. Equipped with active steerable wheels, the four-wheel redundantly-actuated mobile robot (FRMR) allows the main body of wheels and rollers to rotate actively. Thus, it owns higher adaptability to locomote towards arbitrary directions on an uneven floor or slippery terrain [4]. Consensus, precise trajectory tracking of an FRMR performs as the basic foundation that is worthy of effective investigation, especially when the excessive slip, force disturbances and actuator failures at the four wheels cannot be ignored in dynamic environments.

Up to now, many efforts have been devoted to the control design of mobile robots, which can be classified into two categories, i.e., kinematic control and dynamic control [5]–[7]. The kinematic control is widely studied and many good results have been established with the driving wheel velocities being the reference commands [8]–[10]. One prominent advantage of this scheme is that it is not subjected to kinematic model uncertainties, and at the same time, can be used to represent different mobile robots with minor geometric parameter perturbations. However, robotic chassis behaviors are limited due to the fact that the wheel dynamics are not considered when designing a kinematic controller [11]. As is well-known, these parts of dynamics are important since the robot wheels are the means to make it physically reach the objective positions and orientations. In the other side, dynamic control approaches are capable of directly optimizing the driving torques for each wheel such that better anti-disturbance and tracking performances can be expected [12]. For instance, an integrated steering and braking control scheme is presented for automated driving of a vision-based autonomous vehicle, with a special focus on attenuating the coupled and nonlinear features [13]; a cascade motion controller considering actuator dynamics is designed at kinematic and dynamic level simultaneously, which guarantees that the nonholonomic mobile robot tracks

The associate editor coordinating the review of this manuscript and approving it for publication was Okyay Kaynak.

a given trajectory [14]. It is pointed out that most of existing researches concentrate on two/three-wheel, car-like or skid-steered mobile robots, and seldom studies pay attention to a robot platform with redundantly-actuated mechanisms [15], [6]. Meanwhile, wheel-ground interactions are not taken into account during control implementation. This is because formulating an accurate dynamic model of an omnidirectional mobile robot is still a tough work due to complex conditions of external environments with slippery terrain or uneven ground.

Among previous related methods, *Dai et al.* propose a sliding mode control (SMC) that enables a four-wheel-steer four-wheel-drive robot to follow the predefined trajectories [16], [17]. Benefitting from separately regulating each wheel's steer angle, the mobility of an SMC-based robot is improved in narrow spaces [18], [19]. These SMC solutions adopt integer-order (IO) integrator and differentiator to construct a steering sliding surface. As a result, large gain for switching elements is employed leading to serious chattering phenomenon or even fatal damages to the system hardware. Fractional calculus can be extended to eliminate the chattering issue caused by SMC switching principle, especially for the fractional-order (FO) robot systems. It is stated that natural FO features of robot systems have been revealed [20]–[22]. In this sense, an adaptive FO sliding mode control (FOSMC) can help the FRMR to improve its robustness with respect to steering vibration and external disturbances. Due to the additional degree-of-freedom and nonlocality of fractional derivative operators, the FOSMC design is more flexible and useful for dynamic performance shaping during trajectory tracking. However, to the best of our knowledge, the FOSMC has not been applied to dynamic control of the FRMR. In practice, the strong coupling between the position and orientation phases makes it difficult to develop a suitable FO sliding surface which can stabilize the achieved FRMR.

For a dynamic controller of the FRMR, another challenge should be noted is that the online adjustment of multiple driving torques inevitably turns the omnidirectional robot into an over-actuated system. For this end, the allocation principle gives a promising way to schedule good velocity-following performance by formulating an optimization criterion and subsequently deriving applicable control inputs. Recently, works have been done on over-actuated allocation solutions, the applications of which include marine platform, electric vehicle, autonomous underwater vehicle [23]–[25]. Associating with skid-steered mobile robots, *Liao et al.* develop a model-based coordinated adaptive robust controller to address over-actuated features by adjusting the driving torques online [9], [26]. However, actuator failure is not addressed in these allocation solutions. For the FRMR considered in this paper, independent four-wheel control provides advantages such as simple mechanical structure and redundant tire forces. The increased system complexity and the number of actuators also increase the probability of fault occurrences. For instance, the motors (actuators) may also be totally lost, either free-rolling with no power or being locked in a fixed position that results in frictions between the locked wheels and the ground. The faults in the wheel motor result in the performance loss of maneuverability and steering or even lead to system catastrophic failures [27]. On the other hand, the dynamic torque optimization brings heavy calculation burden due to the nonlinearity, non-differentiability and multiple optima requirements of the FRMR control system. Consequently, an efficient allocation controller with fault accommodation capacity is worth exploring to maintain the tracking control performance of the FRMR.

Bearing the above-mentioned analysis in mind, the aim of this paper is to explore an effective fault-tolerant dynamic control (FTDC) for the developed FRMR to keep it functional even if the actuator fault occurs. The main contributions of this paper are fourfold: (1) Compared with conventional kinematic control designs, the FTDC keeps the steering control relatively independent of velocity control, and directly generate the desired driving torques for each wheel to achieve control satisfaction and over-actuated feasibility for the FRMR, despite the actuator failures; (2) Instead of exploiting integer calculus, a novel FOSMC with fractional-integral sliding surface is presented for accurate steering control with enhanced abilities of mitigating the chattering phenomenon; (3) An enhanced artificial bee colony (ABC) is incorporated into the developed FTDC scheme, which is beneficial for guarantying the driving torque optimization efficiency; (4) Implemented on a developed real-time FRMR, comprehensive experiments substantiate the efficacy and superiority of the proposed FTDC trajectory tracking method.

The remainder of this paper is structured as follows. Section II gives the preliminaries and problem statement. The FTDC framework is detailed in Section III, including FOSMC steering regulation and over-actuated optimization solution. Extensive experimental verifications are illustrated in Section IV, respectively. Finally, Section V concludes this paper.

II. PRELIMINARIES AND PROBLEM STATEMENT

A. PRELIMINARIES

There exists two widely-employed fractional operators: Caputo fractional operators and Riemann-Liouville (R-L) fractional operators. It is well-known that R-L fractional operator has initial value problems, therefore Caputo fractional definition is used throughout the whole paper, which is more practical than R-L fractional operator for physical systems.

Definition 1: With an order $\alpha \in \mathbb{R}$, Caputo fractional derivative of a time-dependent function $x(t)$ is given by

$$ {}_{a}^{C}D_{t}^{\alpha}x(t) = \begin{cases} \dfrac{1}{\Gamma(m-a)}\displaystyle\int_{0}^{t} \\ \quad \times \dfrac{x^{(m)}(\tau)}{(t-\tau)^{\alpha-m+1}}d\tau, & m-1 < \alpha < m \\ \dfrac{d^{m}}{dt^{m}}x(t), & \alpha = m \end{cases} \quad (1) $$

where $m \in \mathbb{N}^+$ denotes the first integer that is not less than α, a and t denote the upper limit and lower limit, respectively, $\Gamma()$ denotes Gamma function defined as

$$\Gamma(\alpha) = \int_0^\infty v^{\alpha-1} e^{-v} dv \tag{2}$$

In this paper, a simplified D^α is used to denote ${}_a^C D_t^\alpha$ without any confusion.

Property 1: For arbitrary fractional orders $\alpha, \beta \in \mathbb{R}^+$, the following equalities hold

$$D^\alpha \left[D^\beta x(t)\right] = D^{\beta+\alpha} x(t) \tag{3}$$

$$D^\alpha \left[D^{-\beta} x(t)\right] = D^{\alpha-\beta} x(t) \tag{4}$$

$$D^{-\alpha} \left[D^\beta x(t)\right] = D^{\beta-\alpha} x(t) - \sum_{j=1}^{m} \left[D^{\beta-j} x(t)\right]_{t=t_0} \frac{(t-t_0)^{\alpha-j}}{\Gamma(1+a-j)} \tag{5}$$

where t_0 denotes the start time.

Lemma 1: If there exists a continuously differential function $V(x(t)) \in \mathbb{R}$ with respect to $x(t)$ such that [28]

$$\alpha_2 \|x(t)\|^a \le V(x(t)) \le \alpha_1 \|x(t)\|^{ab} \tag{6}$$

$$D^\beta V(x(t)) \le -\alpha_3 \|x(t)\|^{ab} \tag{7}$$

where $t > 0, 0 < \beta < 1, \alpha_1, \alpha_2, \alpha_3, a$ and b are arbitrary positive constants, then, $x(t)$ is global Mittag-Leffler stable.

B. PROBLEM STATEMENT

As depicted in Figure 1, the kinematic model of an FRMR can be constructed with two virtual wheels located on the center line of the main body, namely front wheel and rear wheel. Let (x_t, y_t) and θ_t denoting the robot position and orientation with respect to the reference coordinate frame, respectively. Then, the kinematic dynamics of the FRMR are described by

$$\dot{x}_t = V_l \cos\theta_t \tag{8}$$

$$\dot{y}_t = V_l \sin\theta_t \tag{9}$$

$$\dot{\theta}_t = \frac{V_l}{L_f + L_r}(\tan\delta_f - \tan\delta_r) \tag{10}$$

where V_l is the longitudinal velocity, L_f and L_r denote the distances from wheels to the robot centre of gravity (***CG***) shown in Figure 1, δ_f and δ_r denote steering angles of the front wheel and rear wheel, respectively.

As shown in Figure 1, an error vector $\boldsymbol{E}$ is defined in the global coordinate frame based on $\boldsymbol{CG} = (x_t, y_t, \theta_t)^{\mathrm{T}}$ and the instantaneous tangent line to the reference point $\boldsymbol{P} = (x_r, y_r, \theta_r)^{\mathrm{T}}$. Aligning with the tangent line to the trajectory ***RP*** at $\boldsymbol{P}$, we will consider the following kinematic offset angel

$$\theta_T = \tan^{-1}\left(\frac{T_y - y_t}{T_x - x_t}\right) \tag{11}$$

$$T_x = x_p + |\boldsymbol{I}|\cos\theta_r, \quad T_y = y_p + |\boldsymbol{I}|\sin\theta_r \tag{12}$$

where T_x and T_y denote the moving distances of *X-axis* and *Y-axis* at $\boldsymbol{P}$, respectively, and $|\boldsymbol{I}|$ denotes the vector of unit magnitude.

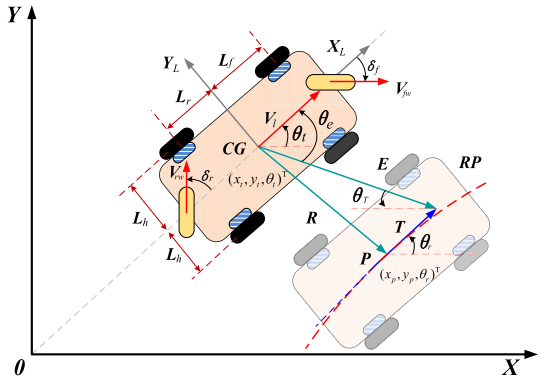

FIGURE 1. Kinematic model of the FRMR.

Define an error signal θ_e determined by $\theta_e = \theta_t - \theta_T$. Then, two measurable virtual states $x_1 = \int \theta_e dt$ and $x_2 = \theta_e$ are presented as

$$\dot{x}_1 = \theta_e = x_2 \tag{13}$$

$$\dot{x}_2 = \dot{\theta}_t - \dot{\theta}_T + d = \frac{V_l}{L_f + L_r}\tan\delta_f - \frac{V_l}{L_f + L_r}\tan\delta_r - \dot{\theta}_T + d \tag{14}$$

where $d = \Delta k_t(\dot{\theta} - \dot{\theta}_T) + d'$ denotes the bounded lumped unknown parameter uncertainties and external nonlinear disturbances, Δk_t represents the uncertainty of the coefficient and d' is the external nonlinear disturbances.

In the other side, the accelerations $\boldsymbol{A}_{ci} = [\, a_{lc} \;\; a_{rc} \;\; \gamma_c \,]^T$ of the developed FRMR is presented as

$$\begin{aligned}\boldsymbol{A}_{ci} &= [\, a_{lc} \quad a_{rc} \quad \gamma_c \,]^T \\ &= \begin{bmatrix} \frac{1}{M-4m_d} & 0 & 0 \\ 0 & \frac{1}{M-4m_d} & 0 \\ 0 & 0 & \frac{1}{J_z} \end{bmatrix} \begin{bmatrix} 1 & 0 & -L_h \\ 0 & 1 & L_f \\ 1 & 0 & L_h \\ 0 & 1 & L_f \\ 1 & 0 & L_h \\ 0 & 1 & -L_r \\ 1 & 0 & -L_h \\ 0 & 1 & -L_r \end{bmatrix}^{\mathrm{T}} \\ &\quad \times \begin{bmatrix} R_1 \boldsymbol{F}_{w1} \\ R_2 \boldsymbol{F}_{w2} \\ R_3 \boldsymbol{F}_{w3} \\ R_4 \boldsymbol{F}_{w4} \end{bmatrix}\end{aligned} \tag{15}$$

where $\boldsymbol{F}_{wi} = [\, F_{di} \;\; F_{Li} \,]^{\mathrm{T}} (i = 1, 2, 3, 4)$ denotes the force vector on the four wheels with F_{di} and F_{Li} being the residual drive force and lateral force, respectively, a_{lc}, a_{rc} and γ_c are the longitudinal, lateral and angular accelerations, respectively, M and J_z are the robot mass and body inertia, separately, m_d is the mass of each driving unit, L_h denotes half of the robot width, $R_i (i = 1, 2, 3, 4)$ is the transfer matrices represented by

$$R_i = \begin{bmatrix} \cos\delta_i & -\sin\delta_i \\ \sin\delta_i & \cos\delta_i \end{bmatrix} \tag{16}$$

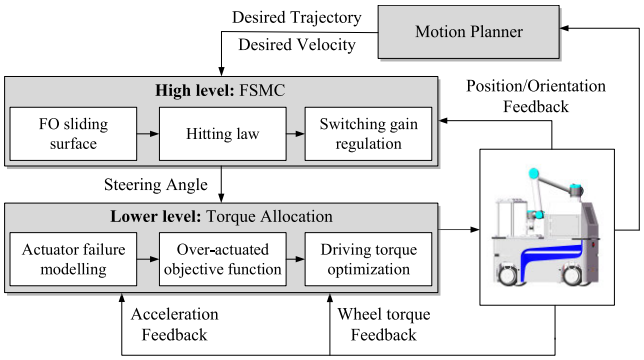

FIGURE 2. Overall control architecture.

where the steering angles $\delta_i (i = 1, 2, 3, 4)$ of four independent wheels are determined by the virtual wheels located in the robotic body center line, i.e.,

$$\delta_i = \tan^{-1}\left(\frac{L_{1i}\tan\delta_f}{L_f + L_{2i}\tan\delta_f}\right) \tag{17}$$

where $L_{11} = L_{12} = L_f, L_{13} = L_{14} = -L_f, L_{21} = L_{24} = -L_h, L_{22} = L_{23} = L_h$.

Based on the kinematic offset model and accelerations formulations of the FRMR, the objective of this paper is to derive the steering anger, i.e., $\delta_i (i = 1, 2, 3, 4)$, and torque control law for the FRMR, referred as an FTDC law. In this way, the actuator failure issue, wheel-ground interactions and wheel dynamics can be properly addressed to keep the FRMR functional and enhance its robustness achieving satisfactory trajectory tracking performance.

III. FAULT-TOLERANT DYNAMIC CONTROL

Aim at obtaining an accurate trajectory tracking, we present an FTDC on the basis of the kinematic and dynamic models of the developed FRMR. As demonstrated in Figure 2, the overall architecture employs a two-level control framework consisting of: (1) a high-level module that determines the desired steering angle so that the instantaneous turning can be derived with guaranteed accuracy; (2) a lower-level module, which accommodates the over-actuated problem by allocating the desired accelerations with optimal torque reference for each wheel to force the developed FRMR to follow the desired velocities precisely.

A. KINEMATIC STEERING REGULATIONS

Differing from the traditional IO relating methods [29], a new FO sliding surface is presented in this paper to enhance the steering convergence and stability

$$s = \sigma_1\theta_e(t) + \sigma_2 D^{\alpha-1}\theta_e(t) \tag{18}$$

where $\sigma_1 \in \mathbb{R}^+$ and $\sigma_2 \in \mathbb{R}^+$ denote user-defined positive coefficients, $\alpha \in (0, 1)$ represents the order of integral operation. It is pointed out that the steady-state error and steering chattering of the resulting robot system can be effectively mitigated by the additional fractional-integral term with pre-defined order α and coefficients $\sigma_i (i = 1, 2)$, as indicated by the following results.

Theorem 1: Suppose the lumped parameter uncertainties and external disturbances are bounded such that $|d| < d_d$ where d_d is a positive constant. The FRMR steering offset model demonstrated by (13) is asymptotically converged if the virtual steering angers δ_f and δ_r are regulated adaptively by applying

$$\begin{aligned}\delta_f &= -\delta_r \\ &= -\tan^{-1}\left(\frac{\left(\sigma_1\dot{\theta}_T - \sigma_2 D^{\alpha}\theta_e(t) - \xi_1 s - \xi_2 sign(s)\right)\left(L_f + L_r\right)}{2\sigma_1 V_l}\right)\end{aligned} \tag{19}$$

where $\xi_1 \in \mathbb{R}^+$ and $\xi_2 \in \mathbb{R}^+$ are switching coefficients and $sign(s)$ is the symbolic function.

Proof: By using (18), we can design the FOSMC system U_{FSMC} expressed as (20), which combines an equivalent control law U_{eq} designed as (21) and a hitting control law U_{hit} designed as (22), i.e.,

$$U_{FSMC} = U_{eq} + U_{hit} \tag{20}$$

$$U_{eq} = \left(\dot{\theta}_T - \frac{\sigma_2 D^{\alpha}\theta_e(t)}{\sigma_1}\right)\frac{L_f + L_r}{V_l} \tag{21}$$

$$U_{hit} = -\frac{L_f + L_r}{\sigma_1 V_l}\left(\xi_1 s + \xi_2 sign(s)\right) \tag{22}$$

Suppose that the control input is determined by $\tan\delta_f - \tan\delta_r = U_{FSMC}$, we get

$$\begin{aligned}\tan\delta_f - \tan\delta_r = &\left(\dot{\theta}_T - \frac{\sigma_2 D^{\alpha}\theta_e(t)}{\sigma_1}\right)\frac{L_f + L_r}{V_l} \\ &- \frac{L_f + L_r}{\sigma_1 V_l}\left(\xi_1 s + \xi_2 sign(s)\right)\end{aligned} \tag{23}$$

Differentiating (18) in time-domain yields

$$\begin{aligned}\dot{s} &= \sigma_1\dot{\theta}_e(t) + \sigma_2 D^{\alpha}\theta_e(t) \\ &= \sigma_1\left(\lambda\left(\tan\delta_f - \tan\delta_r\right) - \dot{\theta}_T + d\right) + \sigma_2 D^{\alpha}\theta_e(t)\end{aligned} \tag{24}$$

The combination of (20) and (24) results in

$$\begin{aligned}\dot{s} &= \sigma_1\left(\lambda\left(U_{eq} + U_{hit}\right) - \dot{\theta}_T + d\right) + \sigma_2 D^{\alpha}\theta_e(t) \\ &= \sigma_1\lambda\left(\dot{\theta}_T\lambda^{-1} - \frac{\sigma_2\lambda^{-1}D^{\alpha}\theta_e(t)}{\sigma_1} - \frac{\xi_1 s + \xi_2 sign(s)}{\sigma_1\lambda}\right) \\ &\quad - \sigma_1\dot{\theta}_T + \sigma_1 d + \sigma_2 D^{\alpha}\theta_e(t) \\ &= \sigma_1\left(-\frac{\sigma_2 D^{\alpha}\theta_e(t)}{\sigma_1} - (\sigma_1)^{-1}\left(\xi_1 s + \xi_2 sign(s)\right) + d\right) \\ &\quad + \sigma_2 D^{\alpha}\theta_e(t) \\ &= \sigma_1 d - \xi_1 s - \xi_2 sign(s)\end{aligned} \tag{25}$$

where $\lambda = V_l(L_f + L_r)^{-1}$ is a defined intermediate variable.

Then, we choose a Lyapunov function candidate as

$$V = 0.5s^2 \tag{26}$$

By applying (25) and (26), we have

$$\dot{V} = s \times \dot{s}$$

$$= s \times (-\xi_2 sign(s) + \sigma_1 d - \xi_1 s)$$
$$= -\xi_2 |s| + \sigma_1 ds - \xi_1 s^2 \quad (27)$$

Thus, if the uncertainties are bounded and the inequality

$$\xi_2/\sigma_1 > d_d \Rightarrow \xi_2 > \sigma_1 |d| \Rightarrow \xi_2/\sigma_1 > |d| \quad (28)$$

is satisfied, the following formulation holds

$$\dot{V} \leq -(\xi_2 - \sigma_1 d_d)|s| \quad (29)$$

From (29), it is concluded that $\dot{V} < 0$ holds, and thus the Lyapunov stability of the closed-loop mobile system is guaranteed, i.e., the reaching condition of sliding mode controller is satisfied. Here completes the proof. □

Theorem 2: The steering regulation law (19) drives the system to converge to switching manifold in finite time.

Proof: Since the hitting law is determined by (22), when $s \geq 0$, the switching manifold becomes

$$\dot{s} = -\frac{L_f + L_r}{\sigma_1 V_l}(\xi_1 s + \xi_2) \quad (30)$$

From (30), we can get the convergence time as

$$t = t_0 - \frac{\sigma_1 V_l \xi_1}{L_f + L_r} \ln \frac{\xi_2}{\xi_1 s(t_0) + \xi_2} \quad (31)$$

where t_0 is the initial time and $s(t_0)$ is the initial state.

Likewise, when $s < 0$, one can obtain that

$$t = t_0 - \frac{\sigma_1 V_l \xi_1}{L_f + L_r} \ln \frac{\xi_2}{-\xi_1 s(t_0) + \xi_2} \quad (32)$$

Thus, if the following inequality with respect to time

$$t \geq t_0 - \frac{\sigma_1 V_l \xi_1}{L_f + L_r} \ln \frac{\xi_2}{\xi_1 |s(t_0)| + \xi_2} \quad (33)$$

is satisfied, the resulted system will converge to the switching manifold in finite time at any initial state. Here completes the proof. □

Theorem 3: The steering error will asymptotically slide to zero under the proposed steering control scheme, i.e., when the sliding mode occurs, the states can converge to the reference points fast and stably.

Proof: When the sliding mode occurs, i.e., $s = 0$, we conclude

$$D^{\alpha-1}\theta_e(t) = -\sigma_1 \sigma_2^{-1} \theta_e(t) \quad (34)$$

Based on property 1, taking the fractional differential of (34) with order $(1-\alpha)$ yields

$$D^{1-\alpha} D^{\alpha-1} \theta_e(t) = D^{1-\alpha}\left(-\sigma_1 \sigma_2^{-1} \theta_e(t)\right) \quad (35)$$

For $\alpha = n$, where n is an integer, the operation $D^\alpha x(t)$ gives the same result of IO integration and differentiation, and specially for $\alpha = 0$, we may obtain $D^0 x(t) = x(t)$ [30]. Thus, one can obtain

$$D^{1-\alpha}\theta_e(t) = -\sigma_1^{-1}\sigma_2 \theta_e(t), \quad 0 < \alpha < 1 \quad (36)$$

Selecting a Lyapunov function candidate in the form of $V = \|\theta_e(t)\|$, its derivative along the trajectory (36) is achieved as

$$D^{(1-\alpha)} V = D^{(1-\alpha)} \|\theta_e(t)\| \quad (37)$$

Then, as studied in [31], one can conclude that the following inequality $D^{(1-\alpha)} \|\theta_e(t)\| \leq sign(\theta_e(t)) D^{(1-\alpha)} \theta_e(t)$, and further we get

$$D^{(1-\alpha)} \|\theta_e(t)\| \leq sign(\theta_e(t)) D^{(1-\alpha)} \theta_e(t)$$
$$= -\sigma_1^{-1}\sigma_2 sign(\theta_e(t)) \theta_e(t)$$
$$= -\sigma_1^{-1}\sigma_2 \|\theta_e(t)\| \quad (38)$$

Then, we may conclude that

$$V + \sigma_1^{-1}\sigma_2 D^\upsilon V \leq 0 \quad (39)$$

From Lemma 1, $\|\theta_e(t)\| = 0$ is globally Mittag-Leffler stable. Therefore, the error signal $\theta_e(t)$ decays towards 0, i.e., $\|\theta_e(t)\| \to 0 (t \to +\infty)$, therefore it is known that the steering control system is asymptotically stable, and the resulting orientation can converge to the reference fast and stably. Here completes the proof. □

In this paper, the symmetric constraint $\delta_f = -\delta_r$ is used in this paper, which implies that the turning radius of the vehicle can be reduced up to 35% by using four-wheel symmetric steering system without crossing the practical limitations [32]. Note that the repeated switching of the sliding surface raises chattering and the gains of the hitting law, that is, ξ_1 and ξ_2, determines the chattering intensity. However, a balance need to be made between the dynamic tracking and chattering elimination, and the system robustness cannot be guaranteed. The slope coefficients of the switching surfaces are regulated adaptively by using the elements of fuzzy logic rules and then achieving the suitable hitting gains. To be more specific, the sliding surfaces s and its differential are the inputs, and $\xi_i (i = 1, 2)$ is chosen as the output. We construct the fuzzy sets as {*Negative Big*, *Negative Small*, *Zero*, *Positive Small*, *Positive Big*}. Then, the type of fuzzy rules is determined by "IF-THEN" using the following form:

$R^{(j)}$: *IF* s is F_s^j and $\dot{s}$ is $F_{\dot{s}}^j$ *THEN* ξ_i is $F_{\xi_i}^j$

where F_s^j and $F_{\dot{s}}^j$ comprise the set of s and $\dot{s}$, respectively, and $F_{\xi_i}^j$ is the output of the j th fuzzy rule.

The aggregate fuzzy output sets for the defuzzification process is converted to precise variables, which is derived by the singleton fuzzifier and center average defuzzifier as

$$output(\xi_i) = \frac{\sum_{j=1}^{m} \left(\gamma_{\xi_i}^i \mu_{F_i^j}(x)\right)}{\sum_{j=1}^{m} \mu_{F_i^j}(x)} = \boldsymbol{H}_{\xi_i}^{\mathrm{T}} \chi_{\xi_i}(x) \quad (40)$$

where $\mu_{F_i^j}(x_i)$ is the Gaussian membership function of linguistic variable x_i, m and n denote the number of fuzzy rules, $\boldsymbol{H}_{\xi_i} = [\gamma_{\xi_i}^1, \gamma_{\xi_i}^2, \ldots, \gamma_{\xi_i}^m]^{\mathrm{T}}$, $\gamma_{\xi_i'}^i$ is the mean value of $\mu_{F_i^j}(x_i)$, $\chi_{\xi_i}(x) = [\chi_{\xi_i}^1(x), \chi_{\xi_i}^2(x), \ldots, \chi_{\xi_i}^m(x)]^{\mathrm{T}}$ denotes the vector of

the height of the membership functions of *output*(ξ_i), and $\chi^j_{\xi_i}(x)$ is defined as

$$\chi^j_{\xi_i}(x) = \frac{\mu_{F_i^j}(x)}{\sum_{j=1}^{m} \mu_{F_i^j}(x)} \tag{41}$$

By using the above fuzzy logic system, the control gain can be scheduled online via the fuzzy rules according to the variety of slding surface and its differential.

For the proposed FOSMC method, the IO case is still applicable. The following results demonstrate the advantages of the proposed FOSMC in terms of the chattering alleviation and control convergence. When the sliding mode occurs, we have

$$\theta_e(t) = E_{1-\alpha,1}(t)\theta_e(0) \tag{42}$$

where $E_{1-\alpha,\beta}(t) = \sum_{k=0}^{\infty} (\sigma_1^{-1}\sigma_2 t^{(1-\alpha)k} / \Gamma((1-\alpha)k+\beta)))$ is the state transfer function [33].

Specially, the state transfer function of IO sliding surface, namely, $1-\alpha = 1$, is determined by

$$\begin{aligned} E_{1,1}(t) &= \sum_{k=0}^{\infty} \frac{-\sigma_1^{-1}\sigma_2 t^k}{\Gamma(k+1)} \\ &= \sum_{k=0}^{\infty} \frac{-\sigma_1^{-1}\sigma_2 t^k}{k!} = \exp(-\sigma_1^{-1}\sigma_2 t) \end{aligned} \tag{43}$$

The decaying type of FO system is different from the IO system. As illustrated in [34], we may get

$$E_{1-\alpha,1}(t) = \sum_{k=0}^{\infty} \frac{-\sigma_1^{-1}\sigma_2 t^{(1-\alpha)k}}{\Gamma((1-\alpha)k+1)} \approx \frac{(-\sigma_1^{-1}\sigma_2) t^{\alpha-1}}{\Gamma(\alpha)} \tag{44}$$

As shown in Figure 3, it can be seen that the state $\theta_e(t)$ of FO system decays towards zero like $t^{-\alpha}$ and IO system decays towards zero like $\exp(-\sigma_1^{-1}\sigma_2 t)$. It proves that the energy transfer is slower with FO sliding surface than that with its IO counterpart. Thus, the inevitable chattering can be mitigated significantly by utilizing the proposed FOSMC steering control method.

B. OVER-ACTUATION SOLUTION

The considered actuator failure is that some motors totally lose power or are stuck which will introduce additional fractions. In this paper, this type of actuator failure for one motor is modelled as

$$F'_{di}(t) = \eta_i(t)F_{di}(t) + (1-\eta_i(t))\,\bar{u}_i(t), \quad t > t_i \tag{45}$$

where i denotes the number of the hub-motor, t_i is the occurring time instant, $\bar{u}_i(t)$ is the friction value that is unknown but constant, and $\eta_i(t)$ is the failure pattern index defined as

$$\eta_i(t) = \begin{cases} 0 & \text{if the } i\text{th motor fails} \\ 1 & \text{otherwise} \end{cases} \tag{46}$$

Note that $\eta_i(t) = 0, \bar{u}_i(t) = 0$ implies that the motor loses its power but can residual rotate freely; $\eta_i(t) = 0$, $\bar{u}_i(t) \neq 0$ means that the motor is stuck that introduces a additional friction $\bar{u}_i(t)$ and counter electromotive force.

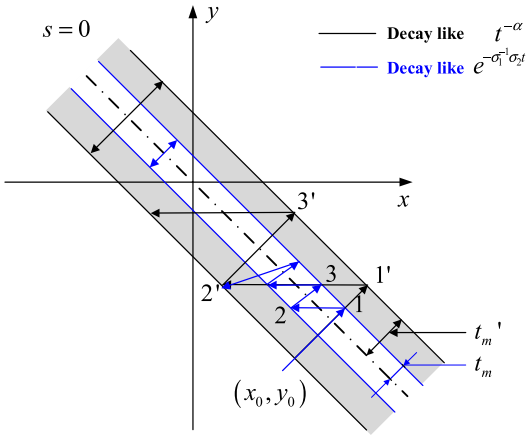

FIGURE 3. Sliding model motion with FO or IO sliding surface.

In this paper, the robot is considered to be functional in steering control due to that the tuning angler and the tuning torque is usually considered to be relatively small. As demonstrated in [16], the lateral force F_{Li} has a linear relationship with the slip angle α_i with $[-5^o \ 5^o]$, so that we obtain $F_{Li} = k_{Li}F_{Ni}\alpha_i$, otherwise $F_{Li} = 5\text{sign}(\alpha_i)k_{Li}F_{Ni}$, where k_{Li} and F_{Ni} are the lateral slip coefficient and vertical load at each wheel, separately. From the kinematic states and geometry relationship of the wheel dynamics, one can derive that

$$\alpha_i = \beta_i - \delta_i = \tan^{-1}\left(\frac{\upsilon_{YV} + l_i\omega}{\upsilon_{XV} + L_i\omega}\right) - \delta_i \tag{47}$$

where β_i denotes the side slip angle indicating the direction of wheel actual velocity $\upsilon_{\omega i}$, υ_{YV}, υ_{XV} and ω denote the longitudinal velocity, lateral velocity and angular velocity, respectively, and $l_1 = l_2 = l_f, l_3 = l_4 = -l_f, L_2 = L_3 = L_h$, $L_1 = L_4 = -L_h$.

As for the residual drive force F_{di}, it is assumed to be linear with the longitudinal slip λ_i, and the slop of this linear relationship depends on the vertical load F_{Ni} and the longitudinal slip coefficient k_{li}, i.e.,

$$F_{di} = k_{li}F_{Ni}\lambda_i = \frac{k_{li}F_{Ni}\,(R_\omega\omega_i - \upsilon_{\omega i})}{\max\{R_\omega\omega_i, \upsilon_{\omega i}\}} \tag{48}$$

where R_ω denotes the wheel radius, $\upsilon_{\omega i}$ denotes the actual longitudinal velocity at the wheel center determined by

$$\upsilon_{\omega 1} = \begin{bmatrix} V_l - L_h\Omega & V_r + L_f\Omega \end{bmatrix} \begin{bmatrix} \cos\delta_1 & \sin\delta_1 \end{bmatrix}^{\mathrm{T}} \tag{49}$$

$$\upsilon_{\omega 2} = \begin{bmatrix} V_l + L_h\Omega & V_r + L_f\Omega \end{bmatrix} \begin{bmatrix} \cos\delta_2 & \sin\delta_2 \end{bmatrix}^{\mathrm{T}} \tag{50}$$

$$\upsilon_{\omega 3} = \begin{bmatrix} V_l + L_h\Omega & V_r - L_r\Omega \end{bmatrix} \begin{bmatrix} \cos\delta_3 & \sin\delta_3 \end{bmatrix}^{\mathrm{T}} \tag{51}$$

$$\upsilon_{\omega 4} = \begin{bmatrix} V_l - L_h\Omega & V_r - L_r\Omega \end{bmatrix} \begin{bmatrix} \cos\delta_4 & \sin\delta_4 \end{bmatrix}^{\mathrm{T}} \tag{52}$$

For each wheel, $\omega_i (i = 1, 2, 3, 4)$ can be obtained by the integration of $\dot{\omega}_i$

$$J_w\dot{\omega}_i = T_i - R_w \begin{bmatrix} \cos\delta_i & \sin\delta_i \end{bmatrix} \begin{bmatrix} F_{di} & F_{ri} \end{bmatrix}^{\mathrm{T}} \tag{53}$$

$$F_{ri} = F_{Ni}k_{ri} \tag{54}$$

where J_w denotes the wheel inertia, T_i is the wheel torque, R_w denotes the wheel radius and k_{ri} denotes the rolling resistance coefficient.

As the controlled robot is an over-actuated mobile robot, construct the following objective function

$$J(\boldsymbol{F}_{wi}) = \min_{F_{wi}} \mu_1(\boldsymbol{A}_{ci}^d - \boldsymbol{A}_{ci}^f)^2 + \mu_2 \|\boldsymbol{F}_{wi}\|^2 + \mu_3 \|\Delta \boldsymbol{F}_{wi}\|^2 \tag{55}$$

where $\Delta \boldsymbol{F}_{wi}$ denotes the driving torque increment, $\boldsymbol{A}_{ci}^d$ and $\boldsymbol{A}_{ci}^f$ denote the desired acceleration deriving from optimizing $\boldsymbol{F}_{wi}$ and acceleration feedback, respectively, $\mu_i (i = 1, 2, 3, 4)$ is the predefined weighting factor.

To find the most suitable force vector, we adopt the ABC algorithm to enhance the optimation efficiency [35], [36]. The ABC algorithm simulates the foraging behavior of bees for multimodal and multi-dimensional numerical optimization problems. This algorithm has numerous advantages of few parameters and strong search capability, which makes it has received large amounts of attention recently. For the traditional ABC, a greedy selection mechanism is applied between the individual x_{ij} and new individual v_{ij}, i.e., $v_{ij} = x_{ij} + rand(0, 1)(x_{ij} - x_{kj})$, where $i = 1, 2 \ldots, SN$, SN is the total number of population, j is uniformly distributed random inter numbers representing the index of each component. In traditional ABC, it should be mentioned that a neighbor of a current individual is selected completely randomly by a current individual to perform the global optimal solution searching of the further iterations. This emplies that efficiency and convergence of the optimization process will be affected since the optimization search is a random search to some extent. Moreover, the achieved solution can easily getting trapped in local monima. As studied in [37], to address this problem, we pick a relatively rational neighbor for the current individual by taking the neighbor information into fully consideration. For this end, we offer the following attractive force F_{ik} of the individual x_k attracting the current individual x_i

$$F_{jk} = G\frac{fit_j \cdot fit_k}{r_{jk}^2 + \varepsilon} \tag{56}$$

where $j = 1, \ldots, SN$, G is the pre-defined attractive force coefficient, $r_{ik} = \|x_i - x_k\|_2$ denotes the Euclidian distance between x_j and x_k, ε is a small constant, fit_j denotes the indicator-based fitness function determined by

$$fit_j = \exp(-J(\boldsymbol{F}_{wi})_j) \tag{57}$$

where $J(\boldsymbol{F}_{wi})_j$ is the cost function value of the solution $\boldsymbol{F}_{wi}$, which is defined as (55).

Moreover, to choose an individual as a neighbor is associated to the attractive force between the current individual and the the neighbor individual. Moreover, for the next iteration, a neighbor individual k can be selected by a current individual i under a probability p_{jk}

$$p_{jk} = \frac{F_{jk}}{\sum_{n=1}^{SN} F_{jn}} \tag{58}$$

The enhanced ABC optimization algorithm related to our over-actuated solution is depicted in **Algorithm 1**. In this way, the optimal driving torques can be obtained for each wheel such that the FRMR can reaching the desired position and orientation.

Algorithm 1 Improved ABC Algorithm

Input: the force vector F_{wi}

Output: over-actuated objective function $J(F_{wi})$

// Initialization
1: Initialize a popution of SN individuals randomly
2:Specifythe related parameters: $limit$, G, ε, α, β, $trail_i$
// the employed bees phase
3: **while** NotExceedMaxIterations **do**
4: **for** each $i \in [1, SN]$ **do**
5: Obtain a new solution v and evaluate its qualty
6: **if** $J(v) \leq J(x_i)$ **then**
7: Replace x_i with v and set $trail_i = 1$
8: **else**
9: Set $trail_i = trail_i + 1$
10: **end if**
11: **end for**
// the onlooker bees phase
12: **for** each $i \in [1, SN]$ **do**
13: Calculate all the probability p_{ik} using (58), $k \in [1, SN]$ and $k \neq i$
14: $r =$ rand(0,1)
15: Find the first j that $p_{i1} + p_{i2} + .. + p_{ij} \geq r$
16: Compute a new solution v and evaluate its qualty
17: **if** $J(v) \leq J(x_i)$ **then**
18: Replace x_i with v and set $trail_i = 1$
19: **else**
20: Set $trail_i = trail_i + 1$
21: **end if**
22: **end for**
// the scout bees phase
23: **for** $i \in [1, SN]$ **do**
24: **if** $trial_s \geq$ limit **then**
25: Replaces x_i with a newly produced individual v
26: Set $trail_s = 1$
27: **end if**
28: **end for**
29: record the best solution obtained so far
30: **end while**

The optimized motor drive forces are the desired residual forces for four wheels. In this paper, we consider the rolling resistance and inertia effects to determine the driving torque $T_i(t)$ applied at individual wheels, which implies

$$T_i(t) = n_g K_t \zeta_g U_i(t), \quad i = 1, 2, \ldots, 4 \tag{59}$$

where $U_i(t)$ denotes the generated current, K_t and n_g denote the torque constant and gear ratio, respectively, and ζ_g is the transmission efficiency between the servo motor and gearbox. To maintain the desired forces on each wheel, proportion

integration controller is applied, which has the advantages of simple structure and easy implementation. However, a proportion integration controller with static parameters cannot achieve a satisfactory control performance. This is because there exist many unknown disturbances such as friction force, time-varying inertia and elastic deformation, which will mitigate the performance of the wheel system. In practice, during the recursive process, the integration cannot achieve tracking capabilities and good static error elimination simultaneously. When the tracking error is small, the PI controller should strengthen the integration factor using a big coefficient to mitigate the static error which may often lead to overshoot or even integration saturation and vice versa. Considering that, we change the traditional proportional-integral controller using an adaptive-scheduled integration rate as

$$U_i'(t) = k_i \left\{ \sum_{i=0}^{t-1} e(i) + f[e(t)]e(t) \right\} T \tag{60}$$

where T denotes the control period, $e(t)$ denotes the force error between the desired force and force feedback, and $f[e(t)]$ denotes the coefficient function determined by

$$f[e(t)] = \begin{cases} 1 & |e(t)| \le B \\ \dfrac{A - |e(t)| + B}{A} & B < |e(t)| \le A + B \\ 0 & |e(t)| > A + B \end{cases} \tag{61}$$

where $A \in \mathbb{R}^+$ and $B \in \mathbb{R}^+$ denote pre-selected constants.

Finally, the input signal for torque control is derived as

$$U_i(t) = k_p e(t) + k_i \left\{ \sum_{i=0}^{t-1} e(i) + f[e(t)]e(t) \right\} T \tag{62}$$

In practice, the limited mechanical properties and saturation nonlinearities of FRMR actuation systems restrict its tracking performance. Meanwhile, higher overshoot, longer regulation time and deteriorative system stability may result from the magnitude constraints. In this paper, the anti-windup approximation of the input signals can be incorporated into the dynamic control framework to further tackle the input saturation issue and enhance the robustness simultaneously [38].

IV. EXPERIMENTAL VERIFICATION

A. EXPERIMENTAL SETUP

To demonstrate the effectiveness and applicability of the proposed FTDC-based method, a real-time implementation of the control strategy is developed for the FRMR for the purpose of performing locomotion and manipulation in industrial manufacturing. Figure 4 demonstrates the main components of the developed FRMR system, which mainly consists of a cooperative manipulator, industrial camera, laser, electric cabinet and four active steer-drive omnidirectional wheels. The on-board industrial computer uses Intel(R) Core (TM) i-74510U processor with a specification of 2.59 GHz and 8G RAM. For the developed FRMR, we can access the torque of the four-wheels directly during the control procedure.

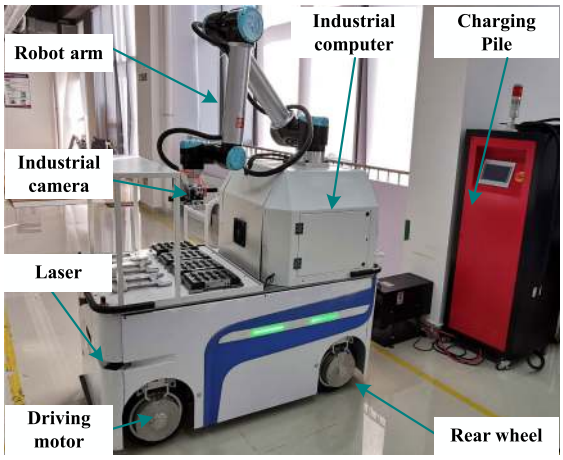

FIGURE 4. The prototype of the developed FRMR.

The parameters of the FRMR are set as $M = 1000\ kg$, $J_z = 60\ kgm^2$, $m_d = 2.352\ kgm^2$, $L_f = 0.48\ m$, $L_r = 0.48\ m$, $L_h = 0.56m$, $J_w = 2.352\ kgm^2$, $R_w = 0.28m$. The robot reduction ratio of the driving axis and steering axis are 7.6 and 60, respectively. The sampling interval is 100 ms. The max steering angle and max torque of the driving motors are 60° and 50 Nm, respectively.

To implement the proposed FTDC method, the corresponding parameters are set as $\xi_1 = 1.25$, $\xi_2 = 4.75$, $\alpha = 0.9$, $k_{ri} = 0.2$, $\xi = 1$, $\mu = 0.001$, $\varepsilon = 0.3$. For comparison, we adopt the traditional kinematic PID control scheme, which calculates the generate control input as velocity terms. Specifically, the parameters of PID controller are determined by $K_p = 1.6$, $K_I = 0.65$ and $K_D = 0.1$.

B. EXPERIMENTAL RESULTS

In order to validate the applicability of the proposed control scheme, the driving torque is optimized and the FRMR is required to follow reference trajectories. Specially, the following three cases are considered to verify the torque optimization efficiency and fault accommodation capacity.

1) CASE 1) TORQUE OPTIMIZATION:

The efficiency comparison is carried out using Matlab 2019 in industrial computer. The related parameters are set as $SN = 200$, $G = 9.8$, $\varepsilon = 0.01$. Figure 5 depicts the running iterations based on the traditional ABC algorithm and the enhanced ABC algorithm. It is clear that the iteration number required for torque optimization is significantly reduced under the enhanced ABC algorithm. As can be seen from Figure 5, the enhanced algorithm can achieve the optimal results within 19 repeated trails while the traditional one needs more than 40 iterations searching for the global optimum. The elapsed time of the traditional ABC is 0.0564 s while after improvement, the required time is reduced to 0.0175 s. This is because that we modify the conventional random search by using an attractive force to drive the current individual to approach the best solution. It is concluded

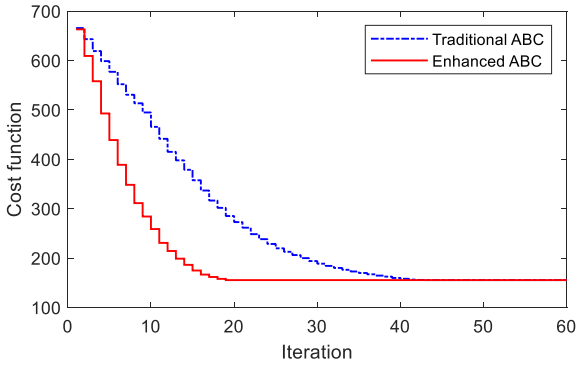

FIGURE 5. Evaluation of enhanced ABC algorithm.

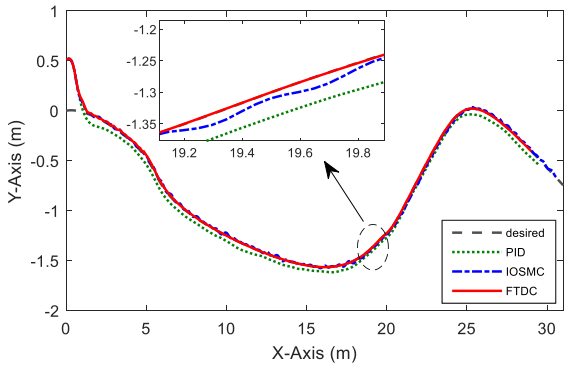

FIGURE 6. Tracking responses of the developed FRMR in case 2.

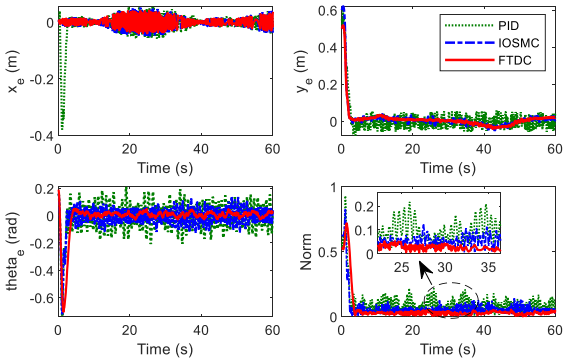

FIGURE 7. Tracking errors of the developed FRMR in case 2.

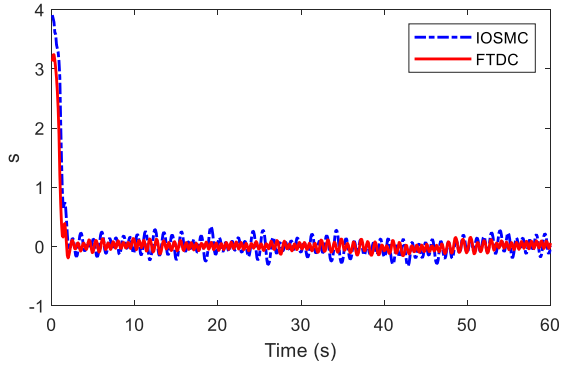

FIGURE 8. The sliding surfaces in case 2.

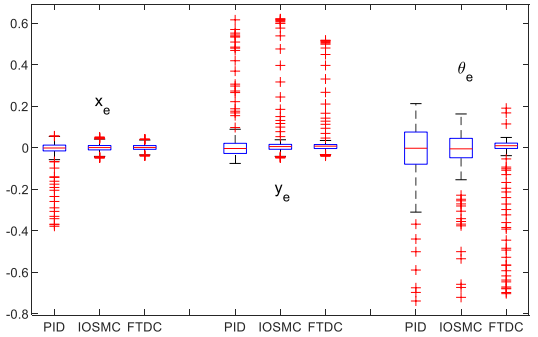

FIGURE 9. Statistics index of the tracking errors in case 2.

that compared with traditional ABC, our enhanced ABC requires less computation time and guarantees optimization efficiency.

2) CASE 2) NORMAL TRAJECTORY PERFORMANCE:

In this case, all the actuators are assumed to be functional during the operational process, which can demonstrate the trajectory tracking performance with respect to steering scheduling and acceleration regulation. The tracking responses and corresponding tracking errors are shown in Figure 6 and Figure 7, respectively. It should be noted that in Figure 7, the norm value of the tracking errors is determined by $\sqrt{x_e^2 + y_e^2 + \theta_e^2}$. As we can see from these results, the FRMR eventually approached the reference trajectory with asymptotic convergence. Moreover, using the proposed FO FTDC scheme, the FRMR is able to mitigate the tracking errors, i.e., x_e, y_e, and θ_e, as comparing to the traditional PID kinematic control and IOSMC scheme. Figure 8 shows the results of the sliding surfaces of IOSMC and the proposed FO sliding surface. It is clear that by utilizing the fractional calculus to construct a sliding surface, the chattering is alleviated significantly, which is useful to enhance the dynamic regulation of the steering angle, thereby achieving smooth trajectory tracking.

To demonstrate the superiors of the proposed method more clearly, we have the performance indexes of the tracking error in terms of the statistics information and integral squared error. The mentioned results are presented in Figure 9 and Figure 10, which show that the new- developed method is capable of obtaining satisfactory performance. As shown in Figure 9, our method makes the tracking error with a smaller vibration around zero, and moreover the average values of these three errors are closer to zero. It is concluded from Figure 10 that under the proposed method the ISE of x_e, y_e, and θ_e are 9.6428 %, 68.4655 %, and 60.9880 % of that under the traditional PID method, respectively. This indicates the effectiveness of our method in a comprehensive way.

Figure 11 and Figure 12 show the steering angles and optimization driving torques on each wheel, respectively, which yields the final trajectory responses above.

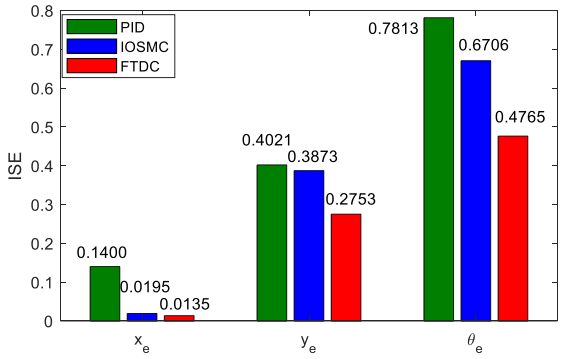

FIGURE 10. ISE of the tracking errors in case 2.

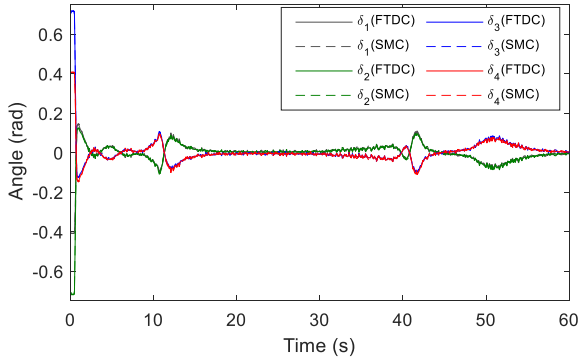

FIGURE 11. Steering angles in case 2.

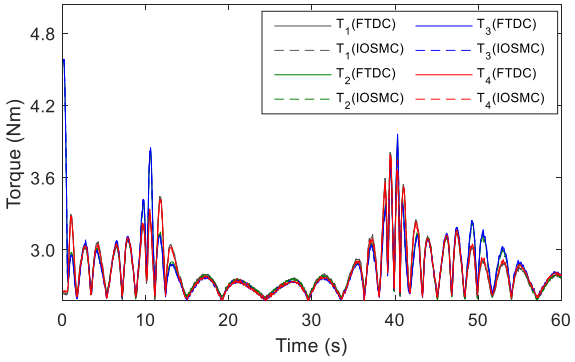

FIGURE 12. Optimized driving torques in case 2.

3) CASE 3) FAULT-TOLERANT PERFORMANCE:

The wheel of number 3 lost its power is considered in this case to evaluate the robustness of the proposed method against actuator failure. The desired trajectory is shown in Figure 13, which is conducted in an uneven ground to supply more disturbances to test the tracking performance. Since the traditional kinematic PID control scheme is not applicable in the presence of actuator failure, we adopt the IOSMC for comparison in this case similarly as case 2.

The experimental results for the fault-tolerant tracking are shown in Figure 13 and Figure 14. Figure 14 is the result of the corresponding tracking errors in which the robot started initial posture errors of 0 m, 0.5 m, 0.4 rad for x_e, y_e, and θ_e, respectively. Although there are forward and backward

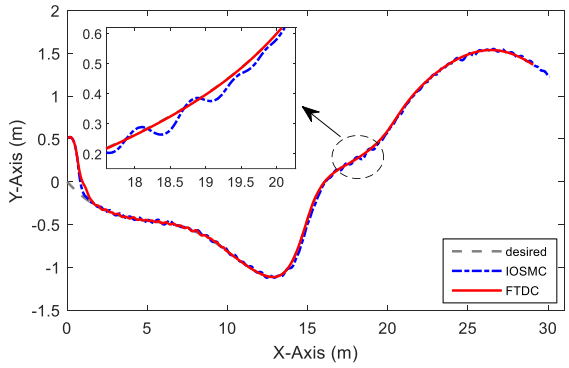

FIGURE 13. Tracking responses of the developed FRMR in case 3.

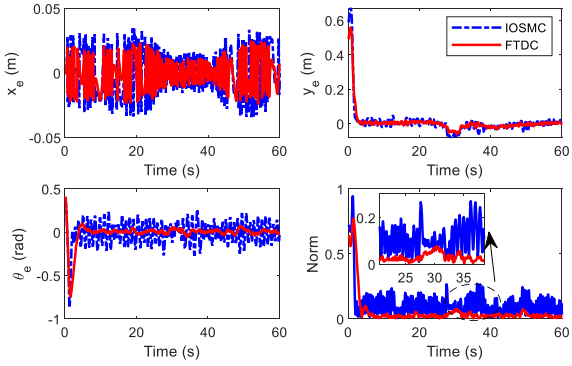

FIGURE 14. Tracking errors of the developed FRMR in case 3.

fluctuations initially in the X-Y directions, all the three posture states converged to desired trajectory. Under the proposed FTDC method, the tracking errors are much smaller as compared to IOSMC method. Specially, as a profile of independently steering regulation, θ_e is mitigated significantly using the proposed FTDC method. Likewise, we present the norm of the tracking errors determined by $\sqrt{x_e^2 + y_e^2 + \theta_e^2}$ in Figure 14, from which we may conclude that our method is of the capacity of enhancing the system dynamic performance comprehensively. It is confined that the proposed FTDC is successful used for the purpose of trajectory tracking of the FRMR in the presence of actuator failure with guaranteed system robustness.

For the designed coupled sliding surfaces, the vibration tendencies are denoted in Figure 15. It is obvious that the sliding surfaces approach zero under the SMC scheme, and some chattering can be found during the sharp tuning of the desired trajectory. With the FO sliding surface, we may mitigate the magnitudes of sliding motions to achieve an acceptable level quickly. Thus, the resulted FRMR system can obtain satisfactory tracking performance.

To be more succinct, we have drawn the performance indexes of the tracking errors with respect to the statistics information and ISE, as shown in Figure 16 and Figure 17, respectively. Compared with the traditional IOSMC scheme, the tracking errors can be significantly reduced by the proposed switched fractional-integral FTDC control scheme.

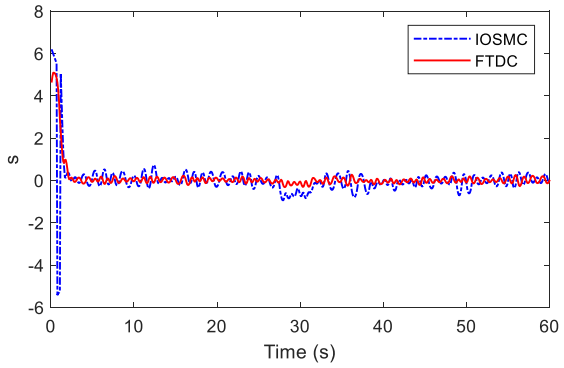

FIGURE 15. The sliding surfaces in case 3.

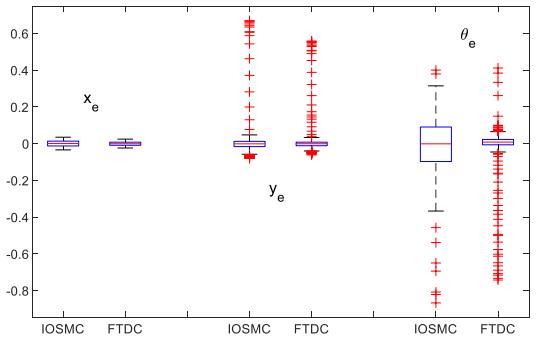

FIGURE 16. Statistics index of the tracking errors in case 3.

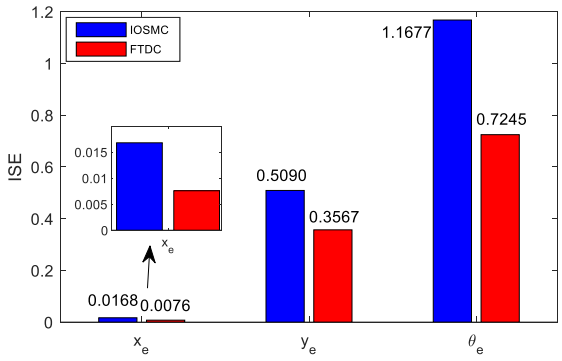

FIGURE 17. ISE of the tracking errors in case 3.

Taking the ISE for example, by using our proposed method, the ISEs of x_e, y_e, and θ_e end up by 54.7619 %, 29.9214 % and 37.9549 %, respectively. This demonstrates that the proposed FO control scheme is beneficial for reducing the tracking error in all the phases due to the additional degree-of-freedom.

Figure 18 and Figure 19 show the steering angles and optimized driving torques of the functional wheels, respectively. It should be mentioned that, in this case, wheel number 3 is assumed to be in fault state with only the ability to roll-freely, which implies it cannot supply power for driving forward or backwards. Thus, comparing with Figure 11, we can see that in this case the control input of T_3 keeps zero during the whole operation. Using our proposed FTDC, both the IOSMC or

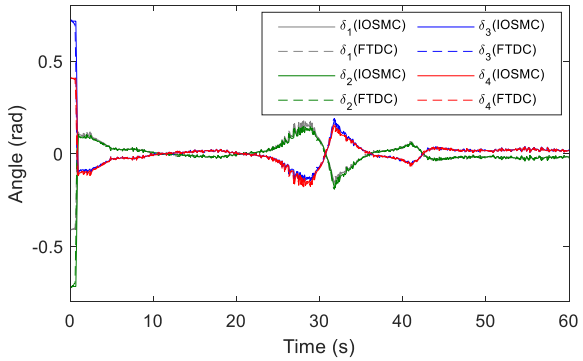

FIGURE 18. Steering angles in case 3.

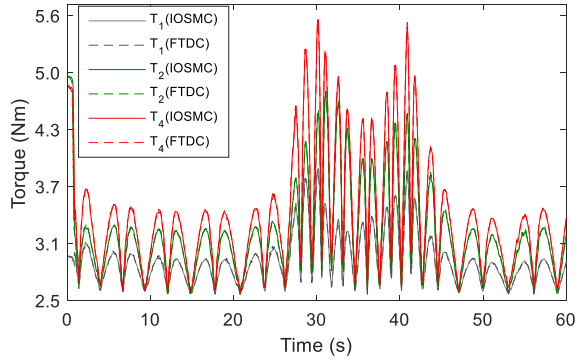

FIGURE 19. Optimized driving torques in case 3.

FOSMC can optimize the torques of the remaining-working wheels to stabilize the FRMR to the desired trajectory. It is shown that the proposed method is robust to the actuator failure, which is more practical than traditional kinematic control schemes that are not useful in such a case.

V. CONCLUSION

In this paper, an FTDC-based dynamic controller had been developed to achieve a robust trajectory tracking of the FRMR with possible actuator failure. Unlike conventional kinematic control, the proposed FTDC-tuned method takes the wheel-ground interactions and wheel dynamics into consideration. The major contributions of this paper lie in a tracking control scheme for the FRMR with fault-tolerant ability to asymptotically stabilize to the desired trajectory. Incorporating fractional calculus into the construction of the sliding surface, the practical FTDC method is potential to independently and accurately enhance the regulation of steering angles. It was shown that, by applying the improved ABC algorithm to optimize the driving torques, the controller behavior of FRMR is robust against over-actuated and actuator failure issues. The proposed method was implemented on a home-developed FRMR system. The experimental comparative results with conventional kinematic PID control method and IOSMC scheme show the superiority of our approach in tracking capability and robustness in the presence of wheel-ground interactions and actuator failure.

Future work can be done on the switching control of the FRMR to accommodate its multiple allocations of kinematic modes, such as diagonal move steer mode, Ackerman mode, skid mode and zero-radius steer mode. By configuring these modes adaptively depending on the desired trajectories and state feedback, the FRMR is able to enhance its capacities of locomotion and manipulation in confined spaces. An autonomous smooth switching mechanism will be focused on to determine the optimal mode, which provides a promising way to achieve improved tracking performance as the FRMR goes further into various applications.

REFERENCES

[1] X. Yang, P. Wei, Y. Zhang, X. Liu, and L. Yang, "Disturbance observer based on biologically inspired integral sliding mode control for trajectory tracking of mobile robots," *IEEE Access*, vol. 7, pp. 48382–48391, 2019.
[2] G. Bai, L. Liu, Y. Meng, W. Luo, Q. Gu, and J. Wang, "Path tracking of wheeled mobile robots based on dynamic prediction model," *IEEE Access*, vol. 7, pp. 39690–39701, 2019.
[3] D. Kim, J. I. Kim, and Y. Park, "A simple tripod mobile robot using soft membrane vibration actuators," *IEEE Robot. Autom. Lett.*, vol. 4, no. 3, pp. 2289–2295, Jul. 2019.
[4] T. Terakawa, M. Komori, K. Matsuda, and S. Mikami, "A novel omnidirectional mobile robot with wheels connected by passive sliding joints," *IEEE/ASME Trans. Mechatronics*, vol. 23, no. 4, pp. 1716–1727, Aug. 2018.
[5] X. Jin, "Fault-tolerant iterative learning control for mobile robots non-repetitive trajectory tracking with output constraints," *Automatica*, vol. 94, no. 8, pp. 63–71, Aug. 2018.
[6] H. Yang, X. Fan, P. Shi, and C. Hua, "Nonlinear control for tracking and obstacle avoidance of a wheeled mobile robot with nonholonomic constraint," *IEEE Trans. Control Syst. Technol.*, vol. 24, no. 2, pp. 741–746, Mar. 2016.
[7] L. Li, Y.-H. Liu, T. Jiang, K. Wang, and M. Fang, "Adaptive trajectory tracking of nonholonomic mobile robots using vision-based position and velocity estimation," *IEEE Trans. Cybern.*, vol. 48, no. 2, pp. 571–582, Feb. 2018.
[8] I. Matraji, "Trajectory tracking control of skid-steered mobile robot based on adaptive second order sliding mode control," *Control Eng. Pract.*, vol. 72, pp. 167–176, Mar. 2018.
[9] J. Liao, Z. Chen, and B. Yao, "Performance-oriented coordinated adaptive robust control for four-wheel independently driven skid steer mobile robot," *IEEE Access*, vol. 5, pp. 19048–19057, 2017.
[10] C. Grand, F. Benamar, and F. Plumet, "Motion kinematics analysis of wheeled–legged rover over 3D surface with posture adaptation," *Mechanism Mach. Theory*, vol. 45, no. 3, pp. 477–495, Mar. 2010.
[11] X. Du, K. K. K. Htet, and K. K. Tan, "Development of a genetic-algorithm-based nonlinear model predictive control scheme on velocity and steering of autonomous vehicles," *IEEE Trans. Ind. Electron.*, vol. 63, no. 11, pp. 6970–6977, Nov. 2016.
[12] Y. Chen, Z. Li, H. Kong, and F. Ke, "Model predictive tracking control of nonholonomic mobile robots with coupled input constraints and unknown dynamics," *IEEE Trans. Ind. Informat.*, vol. 15, no. 6, pp. 3196–3205, Jun. 2019.
[13] J. Guo, P. Hu, and R. Wang, "Nonlinear coordinated steering and braking control of vision-based autonomous vehicles in emergency obstacle avoidance," *IEEE Trans. Intell. Transp. Syst.*, vol. 17, no. 11, pp. 3230–3240, Nov. 2016.
[14] J. Fu, F. Tian, T. Chai, Y. Jing, Z. Li, and C. Su, "Motion tracking control design for a class of nonholonomic mobile robot systems," *IEEE Trans. Syst., Man, Cybern. Syst.*, to be published, doi: 10.1109/TSMC.2018.2804948.
[15] L. Ding, S. Li, H. Gao, C. Chen, and Z. Deng, "Adaptive partial reinforcement learning neural network-based tracking control for wheeled mobile robotic systems," *IEEE Trans. Syst., Man, Cybern. Syst.*, to be published, doi: 10.1109/TSMC.2018.2819191.
[16] P. Dai, "Integration of sliding mode based steering control and PSO based drive force control for a 4WS4WD vehicle," *Autonom. Robots*, vol. 42, no. 3, pp. 553–568, Mar. 2018.
[17] P. Dai and J. Katupitiya, "Force control for path following of a 4WS4WD vehicle by the integration of PSO and SMC," *Vehicle Syst. Dyn*, vol. 56, no. 11, pp. 1682–1716, 2018.
[18] Z. Li, C. Yang, C.-Y. Su, J. Deng, and W. Zhang, "Vision-based model predictive control for steering of a nonholonomic mobile robot," *IEEE Trans. Control Syst. Technol.*, vol. 24, no. 2, pp. 553–564, Mar. 2016.
[19] J. Ni, J. Hu, and C. Xiang, "Robust control in diagonal move steer mode and experiment on an X-by-wire UGV," *IEEE/ASME Trans. Mechatronics*, vol. 24, no. 2, pp. 572–584, Apr. 2019.
[20] J. Chen, B. Zhuang, Y. Chen, and B. Cui, "Diffusion control for a tempered anomalous diffusion system using fractional-order PI controllers," *ISA Trans.*, vol. 82, pp. 94–106, Nov. 2018.
[21] Y. Xie, X. Tang, W. Meng, B. Ye, B. Song, J. Tao, and S. Q. Xie, "Iterative data-driven fractional model reference control of industrial robot for repetitive precise speed tracking," *IEEE/ASME Trans. Mechatronics*, vol. 24, no. 3, pp. 1041–1053, Jun. 2019.
[22] Deepika, S. Kaur, and S. Narayan, "Fractional order uncertainty estimator based hierarchical sliding mode design for a class of fractional order non-holonomic chained system," *ISA Trans.*, vol. 77, pp. 58–70, 2018.
[23] K. Blekas and K. Vlachos, "RL-based path planning for an over-actuated floating vehicle under disturbances," *Robot. Autonom. Syst.*, vol. 101, pp. 93–102, Mar. 2018.
[24] Y. Ma, J. Chen, Y. Peng, and T. Wang, "Simultaneous lateral stability and energy efficiency control of over-actuated electric vehicles," in *Proc. Annu. Amer. Control Conf. (ACC)*, Milwaukee, WI, USA, Jun. 2018, pp. 4733–4738.
[25] K. Tanakitkorn, P. A. Wilson, S. R. Turnock, and A. B. Phillips, "Depth control for an over-actuated, hover-capable autonomous underwater vehicle with experimental verification," *Mechatronics*, vol. 41, pp. 67–81, Feb. 2017.
[26] J. Liao, Z. Chen, and B. Yao, "Model-based coordinated control of four-wheel independently driven skid steer mobile robot with wheel–ground interaction and wheel dynamics," *IEEE Trans. Ind. Inf.*, vol. 15, no. 3, pp. 1742–1752, Mar. 2019.
[27] Y. Ma, V. Cocquempot, M. E. B. E. Najjar, and B. Jiang, "Multidesign integration based adaptive actuator failure compensation control for two linked 2WD mobile robots," *IEEE/ASME Trans. Mechatron.*, vol. 22, no. 5, pp. 2174–2185, Oct. 2017.
[28] J. Wang, C. Shao, and Y.-Q. Chen, "Fractional order sliding mode control via disturbance observer for a class of fractional order systems with mismatched disturbance," *Mechatronics*, vol. 53, pp. 8–19, Aug. 2018.
[29] A. R. Laware, D. B. Talange, and V. S. Bandal, "Evolutionary optimization of sliding mode controller for level control system," *ISA Trans.*, vol. 83, pp. 199–213, Dec. 2018.
[30] S. Pashaei and M. Badamchizadeh, "A new fractional-order sliding mode controller via a nonlinear disturbance observer for a class of dynamical systems with mismatched disturbances," *ISA Trans.*, vol. 63, pp. 39–48, Jul. 2016.
[31] Z. Ding and S. Yi, "Projective synchronization of nonidentical fractional-order neural networks based on sliding mode controller," *Neural Netw.*, vol. 76, pp. 97–105, Apr. 2016.
[32] Y. Xie, X. Tang, B. Song, X. Zhou, and Y. Guo, "Data-driven adaptive fractional order PI control for PMSM servo system with measurement noise and data dropouts," *ISA Trans.*, vol. 75, pp. 172–188, Apr. 2018.
[33] O. Martínez-Fuentes and R. Martínez-Guerra, "A novel Mittag–Leffler stable estimator for nonlinear fractional-order systems: A linear quadratic regulator approach," *Nonlinear Dyn.*, vol. 94, no. 3, pp. 1973–1986, Nov. 2018.
[34] B. Zhang, Y. Pi, and Y. Luo, "Fractional order sliding-mode control based on parameters auto-tuning for velocity control of permanent magnet synchronous motor," *ISA Trans.*, vol. 51, pp. 649–656, Sep. 2012.
[35] B. Akay and D. Karaboga, "A modified artificial bee colony algorithm for real-parameter optimization," *Inf. Sci.*, vol. 192, pp. 120–142, Jun. 2012.
[36] L. Zhang, S. Wang, K. Zhang, X. Zhang, Z. Sun, H. Zhang, M. T. Chipecane, and J. Yao, "Cooperative artificial bee colony algorithm with multiple populations for interval multiobjective optimization problems," *IEEE Trans. Fuzzy Syst.*, vol. 27, no. 5, pp. 1052–1065, May 2019.
[37] W.-L. Xiang, X.-L. Meng, Y.-Z. Li, R.-C. He, and M.-Q. An, "An improved artificial bee colony algorithm based on the gravity model," *Inf. Sci.*, vol. 429, pp. 49–71, Mar. 2018.
[38] Y. Xie, J. Jin, X. Tang, B. Ye, and J. Tao, "Robust cascade path-tracking control of networked industrial robot using constrained iterative feedback tuning," *IEEE Access*, vol. 7, pp. 8470–8482, 2019.

XIAOLONG ZHANG received the master's degree in mechanical engineering from the Huazhong University of Science and Technology (HUST), Wuhan, China, in 2015, where he is currently pursuing the Ph.D. degree with the School of Mechanical Science and Engineering. His research interests include mobile robot, robot control, and motion planning.

YUANLONG XIE received the B.S. degree in electrical engineering and Ph.D. degree in mechanical engineering from the Huazhong University of Science and Technology (HUST), Wuhan, China, in 2014 and 2018, respectively.

He was an Academic Visitor with the School of Electronic and Electrical Engineering, University of Leeds, Leeds, U.K., from 2017 to 2018. He has been a Postdoctoral Fellow with HUST, since November 2018. He has published more than 20 academic journals and conference papers. He holds eight patents. His research interests include robot control, servo control, filed-bus technology, and networked control systems.

LIQUAN JIANG received the B.S. degree in mechanical engineering from the China University of Geosciences, Wuhan, China, in 2014, the M.S. degree in mechanical and electronic engineering from the Huazhong University of Science and Technology, Wuhan, in 2017, where he is currently pursuing the Ph.D. degree with the School of Mechanical Science and Engineering. His research interests include optimization algorithms, robot control, and path planning.

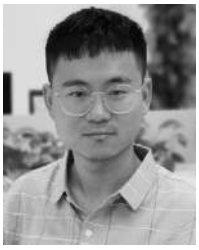

GEN LI received the B.S. degrees in mechanical engineering from the Huazhong University of Science and Technology, Wuhan, China, in 2014, where he is currently pursuing the Ph.D. degree with the School of Mechanical Science and Engineering. He has published ten academic journals and conference papers. His research interests include robot perception, information fusion, and robot programming.

JIE MENG received the B.S. degree in mechanical engineering from the Wuhan University of Technology, Wuhan, China, in 2016. He is currently pursuing the Ph.D. degree with the School of Mechanical Science and Engineering, Huazhong University of Science and Technology, Wuhan. He has published four academic journals and conference papers. He holds two patents. His research interests include robot perception and mobile robot navigation.

YU HUANG received the Ph.D. degree in mechanical engineering from the Huazhong University of Science and Technology (HUST), Wuhan, China, in 2004.

He is currently a Professor with the School of Mechanical Science and Engineering, HUST, where he is also an Assistant Director of the National Engineering Research Center of Manufacturing Equipment Digitization. He has published more than 80 articles. He holds 30 patents. His research interests include mobile robot, mechanical design, and numerical control.